Cross sections and NO product state distributions resulting from substrate mediated photodissociation of NO$_2$ adsorbed on Pd(111)

E. Hasselbrink, S. Jakubith, S. Nettesheim, M. Wolf, A. Cassuto, and G. Ertl

View Online   **Export Citation**

ARTICLES YOU MAY BE INTERESTED IN

Cross sections and NO product state distributions resulting from substrate mediated photodissociation of NO₂ adsorbed on Pd(111)

E. Hasselbrink, S. Jakubith, S. Nettesheim, M. Wolf, A. Cassuto,[a] and G. Ertl

Fritz-Haber-Institut der Max-Planck-Gesellschaft, Faradayweg 4-6, D1000 Berlin 33, West Germany

Ultraviolet irradiation of NO_2 adsorbed on top of a NO saturated Pd(111) surface causes the photodissociation of NO_2/N_2O_4 and results in the desorption of NO molecules. This process has been studied using excitation energies between 3.5 and 6.4 eV. At a photon energy of 6.4 eV, a cross section of 3×10^{-18} cm² is found. Using laser-induced fluorescence to detect the desorbed NO molecules, fully state-resolved data detailing the energy channeling into different degrees of freedom has been obtained. Two desorption channels are found, one characterized by nonthermal state populations, and one showing accommodation to the surface. The yield of the fast channel shows a marked increase above 4 eV photon energy. The slow channel is interpreted as being due to NO molecules which, after formation, undergo a trapping–desorption process. A polarization experiment indicates that the photodissociation is initiated by excitation of metal electrons rather than direct absorption by the adsorbate.

I. INTRODUCTION

Ultraviolet photochemistry of adsorbed molecules has attracted increasing attention in recent years. The rapid growth of the field is stimulated by basic scientific interest as well as by possible technological application in materials processing.[1]

Generally, the absorption of UV photons ($h\nu < 10$ eV) in a polyatomic system may lead to bond breaking (dissociation), which may be envisioned as a composite process, consisting of photon absorption associated with transition to an electronically excited state which may undergo energy redistribution, followed by nuclear motion on a repulsive potential leading finally to dissociation.

Whereas gas-phase photochemistry is a well established and prolific field,[2] the photochemistry of adsorbates is still in its infancy. Compared to the gas phase it is generally expected that excitations might be rapidly quenched due to the coupling to the electron bath in the substrate and that new complexity will arise since the number of degrees of freedom is considerably larger.

In the UV region light absorption can lead to excitation of valence electrons in both the adsorbate and the substrate. When this excitation relaxes into the heat bath of the solid a temperature jump of the surface is caused which might result in processes like thermal desorption. Excitation onto repulsive potential surfaces will, on the other hand, cause the conversion of electronic excitation into translational motion, a process which might be fast enough to escape the quenching.

The exact mechanisms for these processes are still widely unexplored.[3] Besides direct excitations of the adsorbate, photon assisted charge transfer—"hot electron"—processes have been discussed. Studies of NO photodesorption from silicon and gallium arsenide provided evidence for chemically active carriers produced through band gap excitation of the substrate.[4]

Recently it has become evident that photodissociation can in some cases compete effectively with the quenching even on *metal* surfaces especially in the case of weakly bound molecules.

The photodissociation of CH_3Br on LiF has been studied by Bourdon *et al.*[5] and Tabares *et al.*[6] The CH_3 radical shows velocity distributions which are compatible with the energy balance expected for dissociation of the isolated molecules if one takes into account the changed kinematics of the repulsive separation. Marsh *et al.*[7] studied the same process on a metal surface, Ni(111). Here a strong loss of energy to the metal is observed. For CH_3Cl they report that besides direct molecular absorption channels, a charge transfer channel contributes to the methyl ejection.[8]

White and co-workers[9] have studied the formation of photolysis fragments remaining at the surface from several molecules, especially methylhalides and physisorbed oxygen.

Budde *et al.*[10] have reported on the photodesorption of NO from NiO. They estimate a total desorption cross section of 2×10^{-17} cm² for 6.4 eV excitation. Nonthermal state distributions and a pronounced spin–orbit selectivity for molecules with low rotational excitation are observed. Buntin *et al.*[11] have observed the photodesorption of NO from Pt(111). This is the first report of a laser stimulated desorption process from a clean metal surface. From the data given by the authors, we estimate a cross section of about 10^{-22} cm². Further, a marked dependence of the population found in $v = 1$ on the desorption-laser wavelength is reported. Natzle *et al.*[12] looked at the UV-photodesorption of NO from condensed films finding a substantial amount of photochemical desorption and a high degree of vibrational excitation.

Gas phase photodissociation of NO_2 has been studied in great detail by several authors. The absorption of NO_2 and its dimer N_2O_4 in the UV has been measured by Bass *et al.*[13] NO_2 photodissociation exhibits two channels, one asymptotically approaching $NO(X\,^2\Pi)$ and $O(^3P)$ and the other

one yielding $NO(X^2\Pi)$ and $O(^1D)$. The first channel has a threshold at 25 137 cm^{-1} (3.12 eV),[14] whereas the second one becomes energetically open at 40 998 cm^{-1} (5.083 eV). The first is known to produce vibrationally excited NO. Zacharias *et al.*[15] for photodissociation at wavelengths between 351 and 308 nm (3.5 and 4.0 eV), and Slanger *et al.*,[16] for 248 nm (5.0 eV), find vibrational state distributions peaking at the highest accessible vibrational state. The absorption spectrum of NO_2 shows a minimum near the onset of the second channel which is known to produce vibrationally and rotationally cold NO.[17] Taherian *et al.*[18] find for 157 nm (7.9 eV) that the $O(^3P)$ channel is dominant resulting in extensive vibrational excitation. The photodissociation of dimeric NO_2, N_2O_4, has been studied by Kawasaki *et al.*[19] for 193 and 248 nm excitation. The authors report the fragmentation into two NO_2 molecules, at least one being in an excited state.

This paper concerns a study on the release of NO into the gas phase upon photodissociation of NO_2 adsorbed on a Pd(111) surface. This process is initiated by UV-laser radiation in the energy range between 3.5 and 6.4 eV. Due to effective relaxation of electronic excitation of systems strongly coupled to a metallic surface, the cross section for photochemical processes of chemisorbed species are generally very small,[20] but become much higher for weakly held species on nonmetallic substrates. Since NO_2 chemisorbed on Pd(111) will undergo partial (thermal) dissociation into $NO_{ad} + O_{ad}$, which might proceed further due to interaction with radiation, the experiments to be reported here were performed with NO_2 adsorbed on top of a saturated layer of chemisorbed NO. In this way high photodissociation cross sections with a well-defined adsorption system, which allows to run the experiment under steady-state conditions for extended periods of time, were reached.

We report on fully state-resolved measurements with respect to the translational, rotational, vibrational, and spin–orbit energy distribution for the NO molecules desorbing. We observe two channels for the release of NO molecules. One channel exhibits translational energies as well as rotational and vibrational excitation far in excess of those to be expected for a thermal process. Its cross section begins to increase sharply between 4 and 5 eV. The second channel releases NO molecules thermally accommodated with the surface.

By varying angle and polarization of the incident radiation, clear discrimination between two, basically different, mechanisms of primary excitation could be made. It turns out that in our case this consists in electronic excitation of the metallic substrate followed by conversion into valence level excitation of the adsorbate, rather than in direct photoexcitation.

II. EXPERIMENTAL

The apparatus used has been described in detail previously.[21] Therefore it suffices to briefly outline its principle and some of the modifications that have been made for the present work. The experiments were performed in an UHV chamber equipped with a sample manipulator, a combined LEED/AES unit and an Ar$^+$ sputter ion gun. The chamber

also contains a quadrupole mass spectrometer (QMS) which is mounted on a turntable so that it can be rotated around the crystal. A block diagram is given in Fig. 1.

The palladium sample, cut within 0.5° of the (111)-plane, was mounted between a pair of tungsten wires, which were connected to a copper rod making direct contact with a liquid nitrogen reservoir. The sample could be radiatively heated. The temperature was measured by a chromel-alumel thermocouple spot welded to the backside of the crystal. Heating of the crystal was controlled by a feedback circuit in order to keep the temperature constant to within 1 K.

The sample surface was cleaned by standard procedures until no impurities were detectable in the AES spectra. LEED reproduced the known structures for the clean and the NO covered surface.[22]

For irradiation of the sample, an excimer laser (Lambda Physik, EMG150E) is employed as light source. By operating it on the rare gas fluoride mixtures (ArF, KrF, XeF), light at three distinct wavelengths (193, 248, and 351 nm, respectively) can be produced. A second excimer laser (XeCl) produced 308 nm radiation. The duration of the light pulses ranges between 8 and 20 ns for the different gas mixtures used. In all cases the pulse fluence was reduced to typically 5 mJ/cm^2. Based on the equations given by Burgess *et al.*[23] and the optical data given in Ref. 24, the transient temperature rise of the irradiated sample surface induced by this fluence is less than 20 K. Unless otherwise noted, the laser beam was directed perpendicular onto the crystal surface.

The laser output is, under normal conditions, not polarized but, if desired, a Rochon prism was used in order to

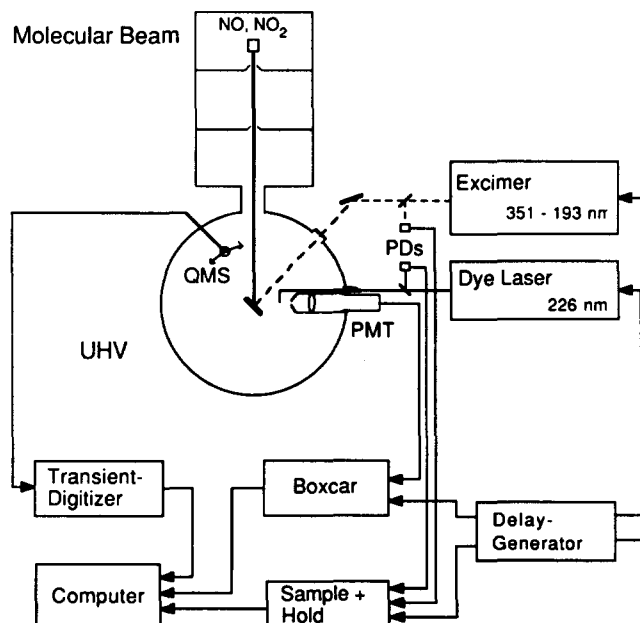
FIG. 1. Schematic of the apparatus and experimental set-up. A pulsed nozzle beam is used to dose the crystal between the laser shots. The quadrupole mass spectrometer (QMS) and the dye laser/fluorescence detection system are used to detect the flux of desorbed molecules. Both systems allow us to record time-of-flight data. Two photodiodes (PD) are used to monitor the pulse power of the lasers.

obtain polarized light. The rotation of this prism selects the plane of polarization.

In the course of these experiments two sets of data were recorded. The rotatable mass spectrometer detects the desorbing molecules independent of their internal state distribution. We will call this data *integral*. Due to the pulsed nature of the laser light which initiates the desorption, it is straight forward to measure time-of-flight (TOF) spectra which reflect the translational energies of the desorbing molecules. The crystal-to-ionizer distance was 80 mm. The NO ion flight time through the quadrupole was assumed to be 15 μs.[25]

State specific data have been obtained using laser-induced fluorescence (LIF) to detect the NO molecules. The frequency doubled output of an excimer pumped pulsed dye laser (Lambda Physik, EMG201E + FL 2002) is tuned through the NO $A\,{}^2\Sigma^+\,(v',J')\leftarrow X\,{}^2\Pi(v'',J'')$ band at 226 nm. The subsequent fluorescence is imaged onto a photomultiplier tube (PMT, EMI 9462). The probe laser intersects the flux of desorbing molecules parallel to the crystal surface and perpendicular to the plane formed by the desorption laser and crystal normal. The point at which this plane is intersected is under 45° with respect to the crystal normal. The distance between the detection volume and the surface—the flight distance of the desorbing molecules—could be varied between 15 and 40 mm, but was typically set at 25 mm. The polarization was set to the "magic angle."

This set-up allows for a nearly complete determination of the state variables of the desorbing NO molecules. Because of the pulsed nature of both laser, only molecules with a specific flight time are detected. By varying the delay between the two laser pulses, state-selected time-of-flight spectra can be recorded. Rotational state distributions were obtained by scanning the wavelength of the probe laser at a fixed time delay. The diameter of the probe laser beam (≈ 3 mm) together with the spatial extension of the sample limit the velocity resolution to $\approx 10\%$.

Scattered light from the desorption laser and fluorescence from diverse mounting parts are a severe problem for LIF detection in this type of experiment. Several efforts were undertaken to overcome this problem. First, the scattered light was suppressed by two sets of reflection filters (Schott UV-R-250) with a maximum transmittance at 250 nm. Second, the PMT was gated by applying an appropriate pulsed voltage to a focusing electrode, which prevented photoelectron emission during the desorption laser pulse. Third, mounting parts close to the crystal were covered with graphite. Unfortunately, because of the overlap with the fluorescence from NO, this set-up does not allow low level LIF detection when the excitation laser is operated at 248 nm.

The (probe) dye laser is operated at moderate output powers so that, in the detection volume, 15 μJ/pulse are generated. It was checked that at this power level no NO transition saturates and photodissociation of gaseous NO₂ is below detection limit.

NO gas was 99% pure from Messer-Griesheim. It was contaminated with NO₂ and N₂O. The NO₂ impurities were removed by flowing the gas through a cold trap held at 150 K. The N₂O impurity could not be removed at this tempera-

ture, but it is of less concern because N₂O does not form a multilayer structure at the applied sample temperatures. NO₂ was 98% pure from Messer-Griesheim. NO was removed by fractional distillation of the NO₂. N₂O₃ was oxidized to NO₂ by bubbling O₂ through the liquid.

The crystal was typically held at a base temperature of 105 K. The first step was to dose the cold substrate with a neat pulsed beam of NO to precover it up to saturation. Subsequently the beam was switched to NO₂. Starting with the NO saturated surface two approaches are possible. First, the crystal can be dosed with a fixed amount of NO₂ yielding a certain coverage. Then this system can be subject to the laser irradiation. The initial desorption signal observed during the first laser shots is then measured. This approach was chosen whenever a constant coverage was desired. The second approach consists in firing the desorption laser and the nozzle synchronously. The nozzle is fired once after each laser shot. After a short time a steady state between laser removal and replacement by the pulsed beam is established. The steady-state coverage is controlled by the open time of the nozzle and could be checked by a subsequent TPD. In order to avoid the build-up of a multilayer structure of NO₂, nozzle and laser firing were started at the same time. The coverage was kept in the range of 0.1–0.2 ML. This approach was chosen for the state-specific and time-of-flight experiments.

Rotational populations N_J were extracted from the LIF spectra by correcting for the line strength, as given by the Hönl–London factors[26] and the degeneracy. The resulting data will be presented as Boltzmann plots of ln N_J vs $E_{J\Omega}$, the rotational energy plus spin–orbit energy. This graph is linear with a slope of $-1/kT_{\mathrm{rot}}$ if the population follows a Boltzmann distribution. However, there is *a priori* no requirement that the data fit this model and T_{rot} is in general no thermodynamic quantity.

The procedure for the quantitative analysis of the TOF spectra has already been described in earlier work.[27] The analysis has to take into account the fact that LIF and mass spectroscopic detection both measure the particle density. But the conversion into fluxes is straight forward. In both representations, the data can be fit using a modified Maxwell–Boltzmann distribution. In the density domain it is formulated as

$$n(t) = at^{-4}\exp\left[-b\left(\frac{d}{t}-v_0\right)^2\right], \qquad (1)$$

where a is a normalization constant, b a measure of the kinetic energy, v_0 a flow velocity, d is the distance between the crystal and the detection point and v is connected to the flight distance and time by $v = d/t$. This formula represents a Maxwell–Boltzmann distribution in a moving reference frame, where v_0 is the common offset velocity. In the observed TOF spectra this shows up as a velocity distribution which exhibits a width different from an ordinary velocity distribution. In general, we will have to use a sum of two of these functions in order to represent the data, because, as will be seen below, we observe usually bimodal velocity distributions. *A priori* there is no justification for a Maxwell–Boltzmann distribution and a reduction to only *two* channels. But, as will be seen, this approach is strongly suggested by the

experimental data and serves as a convenient method to extract the information about average quantities.

The mean translational energy $\langle E_{trans} \rangle$, the mean velocity $\langle v \rangle$, and the variance $\langle \sigma^2 \rangle$ can be derived by numerical integration from the fitted curves. Fitting, in both the density and flux domains, leads to nearly identical results. In the figures we will give the data in terms of fluxes, because then the area under the curves is directly proportional to the fractions of particles branching into the different channels observed.

III. RESULTS

A. Characterization of adsorption states

The adsorption of NO on Pd(111) has been studied by several authors.[22,28] The thermal desorption spectrum [Fig. 2(a)] exhibits three distinct peaks at 257, 288, and 510 K. The high temperature state (γ) is largely disordered without a well-developed LEED pattern. After completion of the $\beta + \gamma$ states a $c(4 \times 2)$ structure is formed, while at saturation ($\alpha + \beta + \gamma$) a (2×2) LEED pattern is observed. Bertolo and Jacobi[29] conducted very recently a combined
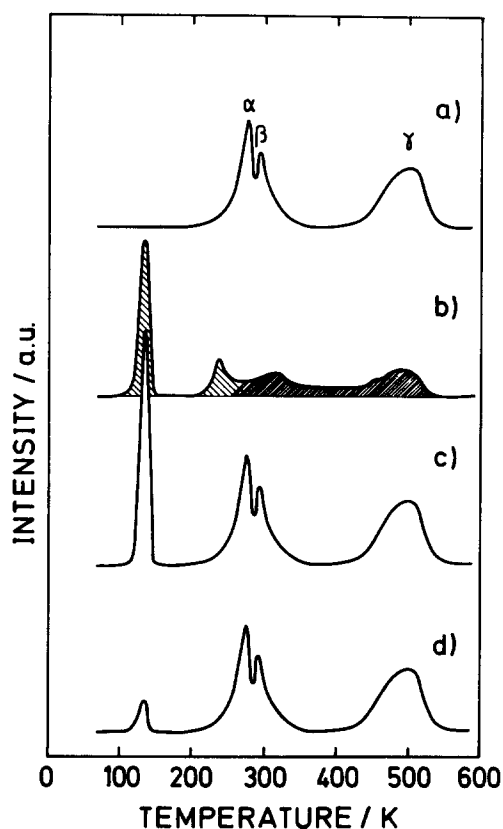

FIG. 2. Temperature programmed desorption (TPD) spectra for NO and NO₂ adsorbed on Pd(111). Trace a depicts the TPD from a saturated coverage of NO. It exhibits three adsorption states for NO chemisorption. Trace b gives the TPD for NO₂ adsorbed on clean Pd(111) after a dose of 3 L. Trace c shows a TPD which is achieved when the crystal is first dosed with NO until saturation is obtained and subsequently 0.6 L of NO₂ are dosed. After this structure has been exposed to 150 laser shots (5 mJ/cm²/pulse) trace d is observed. All spectra have been recorded with the mass spectrometer tuned to mass 30. (NO₂ is recorded with a probability of 60% on this mass.) The heating rate was in all cases 7 K/s.

HREELS and ARUPS study. They propose a model of the saturated layer where NO is bound in bridge and close to atop sites forming a hexagonal structure. The saturation coverage is 3/4 ML.

The adsorption of NO₂ on Pd(111) has not been studied previously. Trace *b* of Fig. 2 shows the temperature programmed desorption (TPD) spectrum for NO₂ after an exposure of 3 L.[30] NO₂ desorbes molecularly around 140 and 230 K. At higher temperatures the desorption of NO is observed indicating that NO₂ partly dissociates either at the temperature of adsorption or while the sample is heated. At higher doses the adsorption state at 230 K is first filled, but before it is saturated a physisorbed species desorbing at 140 K is observed. There is no indication for saturation of this state. Its build-up is linear with exposure and leads to the formation of multilayers. The sticking coefficient is close to unity. Assuming a "normal" frequency factor of 10^{13} s^{-1} one derives for the binding energy of physisorbed NO₂ a value of 0.35 eV. These findings resembles those reported by Bartman *et al.*[31] for NO₂ adsorbed on Pt(111).

The TPD reproduced in trace *c* of Fig. 2 is observed when NO₂ is adsorbed on top of a saturated NO layer. The binding energy for NO₂ is not distinguishable from the one found for the multilayer feature shown in trace *b*. Hence, the interaction between the NO₂ adsorbed on top of a chemisorbed NO layer is energetically not noticeably different from that in a NO₂ multilayer. The same TPD is also observed when a mixture of NO with a small amount of NO₂ is used to dose the crystal. Because the chemisorption energy for NO is larger than that for NO₂ and a larger amount of the first is offered to the surface, NO will occupy nearly all of the surface sites. When these are saturated only NO₂ will further stick and form the multilayer structure. Our data gives no direct indication whether NO₂ forms dimer (N₂O₄) on the surface, but this seems to be highly probable based on the 0.54 eV bond energy of the dimer and its ready formation in the gas and liquid phase.

Any change which might be caused by the overlayer of NO₂ in the binding of NO to the metal surface turns out to be reversible. It can be assumed from the weak interaction that only slight changes are induced by the physisorbed NO₂. On the other hand this implies that the surface becomes passivated by the layer of chemisorbed NO.

After irradiation of such a composite NO₂/NO overlayer with 150 laser shots at 193 nm (5 mJ/cm²/pulse), the TPD reproduced in trace *d* of Fig. 2 is obtained. It is obvious that the amount of NO₂ adsorbed has been reduced, whereas no modification of the NO binding peaks and their population is found. We further note that no other species resulting from photolysis could be detected by post-irradiation TPD.

In order to check for photodesorption of chemisorbed NO we prepared a saturated (2×2) layer and exposed it to laser radiation. We could observe no significant removal of chemisorbed NO under our conditions. This holds even when the crystal base temperature is set close to the thermal desorption maxima of NO at 257 K. Even after an exposure to laser firing (10 Hz) for one hour, no depletion could be detected. This is consistent with the data reported for the NO–Pt(111) system.[11]

B. Cross sections

The last two panels of Fig. 2 point to a method for determining the cross section for NO$_2$ depletion. As will be demonstrated in detail later, this process consists in photodissociation and release of NO into the gas phase, rather than in photodesorption of (intact) NO$_2$ molecules. Starting from a fixed coverage of NO$_2$ on top of a saturated layer of NO, the crystal is exposed to a variable number of laser shots. The residual coverage is afterwards determined by a TPD. The desorption feature from chemisorbed NO and its known coverage serves an internal calibration through comparison of the area under the NO$_2$ feature with that of NO. The coverages derived in this way are given in monolayers (ML), referring to the number of Pd atoms on the (111) surface.[32] If the NO$_2$ removal process follows a simple exponential law, a straight line should be observed in a semilogarithmic graph, with a slope which determines the cross section σ:

$$N = N_0 e^{-\sigma n_{ph}}, \qquad (2)$$

where n_{ph} is the fluence of laser photons.

In Fig. 3 these data are presented for a desorption-laser wavelength of 193 nm. The three curves represent data points obtained starting from different initial NO$_2$ coverages. For the smallest initial coverage of 0.35 ML, we obtain data points which are very well reproduced by an exponential decay law. Because the data has been obtained with a laser fluence of 5 mJ/cm^2 (about 5×10^{15} photons/cm^2) resulting in a removal of only 1% of the coverage per shot, we can interpret the data as a continuous measure of the residual coverage versus number of photons per unit area having impinged on the surface. From the slope of this curve we derive a cross section of 3.1×10^{-18} cm^2.

The good fit of the data over more than one order of magnitude with a single exponential indicates that coverage dependent interactions between the NO$_2$ molecules are without noticeable effect on the desorption probability. Starting from higher initial coverages we observe that for the first laser shots the cross section is higher, but with further irradiation the curves are well represented by a straight line having the same slope as obtained from the fit to the 0.35 ML data. One explanation for the initially higher cross section might well be that the NO$_2$ multilayer structure is at first rough and becomes annealed by the desorption and heating which is coupled with the first laser shots. After this process is completed the curves level off to the same slope. In this regime the cross section is again independent of coverage.

Monitoring the yield of the desorbing NO molecules with the QMS we have extended these measurements to higher coverages (Fig. 4), whereby different steady state converages are established by varying the ratio of the number of nozzle pulses to laser pulses. For 4 and 5 eV excitation we observe, that at first the yield increases linearly with coverage, whereas from 0.54 ML on the curve levels off. This switching point corresponds very well to the estimated coverage of a completed layer of condensed NO$_2$. For 6.4 eV photon energy the region of linear increase extends to higher coverages and the yield levels off as late as 4 ML. The linear region indicates that all layers take part in the desorption process with an equal probability to cause the release of molecules. It must be born in mind that a linear increase with coverage implies a constant cross section for the process. For the other extreme, the constant yield for high coverages indicates that only a limited number of layers release molecules. The difference in the behavior observed for excitation at 6.4 eV and below might well be attributed to the fact that only the 6.4 eV excitation energy is higher than the work function of the NO/Pd(111) system and therefore photoelectrons are produced.
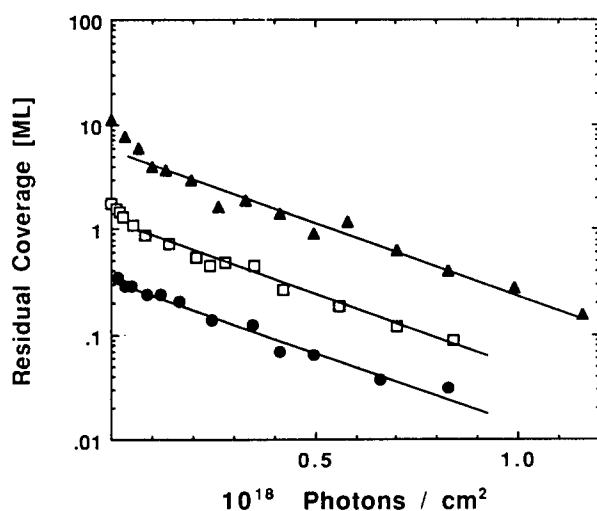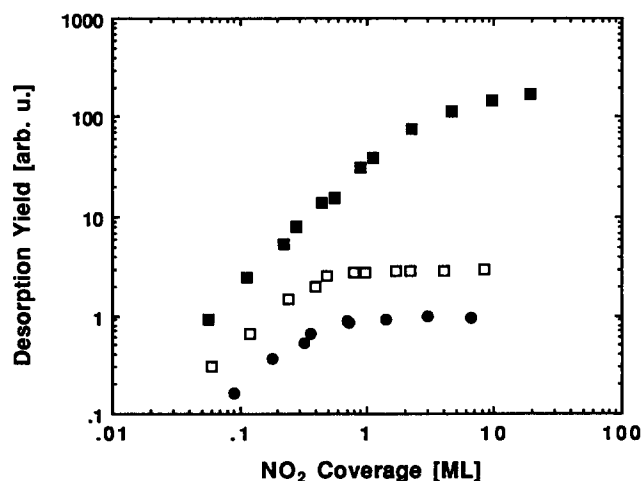

FIG. 3. Residual NO$_2$ coverage versus number of photons impinged onto the surface. Three data sets starting from different initial coverages (●: 0.35 ML; □: 2 ML; and ▲: 11 ML) are shown. The coverages are calibrated with respect to the saturation coverage of NO (0.75 ML). The first set has been fit assuming an exponential decay. A line with the same slope has been drawn for the other data sets and is found to represent these well.

FIG. 4. Desorption yield versus NO$_2$ coverage. For low coverages a linear dependence of the photodesorption yield on the coverage is observed. At higher ends the curve levels off indicating that only the topmost layers contribute to the release of molecules. ■: 193 nm (6.4 eV); □: 248 nm (5.0 eV); and ●: 308 nm (4.0 eV).
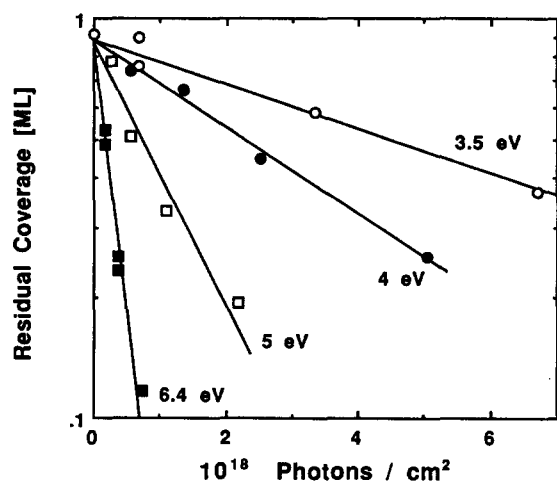
FIG. 5. Layer depletion data for using different photon energies to initiate photodesorption. With decreasing energy a rapid decrease of the desorption cross section is observed. ■: 193 nm (6.4 eV); □: 248 nm (5.0 eV); ●: 308 nm (4.0 eV); and O: 351 nm (3.5 eV).

For the high coverages tested here we do not observe that the yield decreases again as might be expected under the assumption that metal excitations play a significant role in the desorption process. On the other hand, an excitation transfer process might be active which allows to rapidly transfer an excitation once established within the condensed film to the topmost layers.

For now, we set aside the multilayer photochemistry, and will focus solely to condition of submonolayer NO₂ coverages. A detailed study of the photodesorption from condensed mutlilayer films of NO₂ has not been undertaken and is beyond the scope of this work.

Using different gas mixtures in the excimer lasers, the cross section measurements have been extended to study the dependency on photon energy. Figure 5 shows the data for layer depletion using the four available energies in the range of 3.5 to 6.4 eV. The decrease of the slope indicates a decrease of the cross section with longer wavelength. Based on these

data we derive cross sections which vary by more than an order of magnitude (Fig. 6). The values obtained for 3.5 and 4.0 eV are not markedly different. Going to 5.0 eV a marked increase is observed, which continues to 6.4 eV for which the highest value is found. Unfortunately no shorter wavelength radiation was available.

The optical absorption coefficient of Pd in this wavelength region (Fig. 6) changes only by a factor of 1.5, from 0.41 to 0.63. Therefore, by itself, it can not explain the observed pronounced increase of the cross section above 4 eV.

We have checked the dependence of the yield on the laser fluence. In the range from 2 to 70 mJ/cm² we find a linear dependence for both channels.
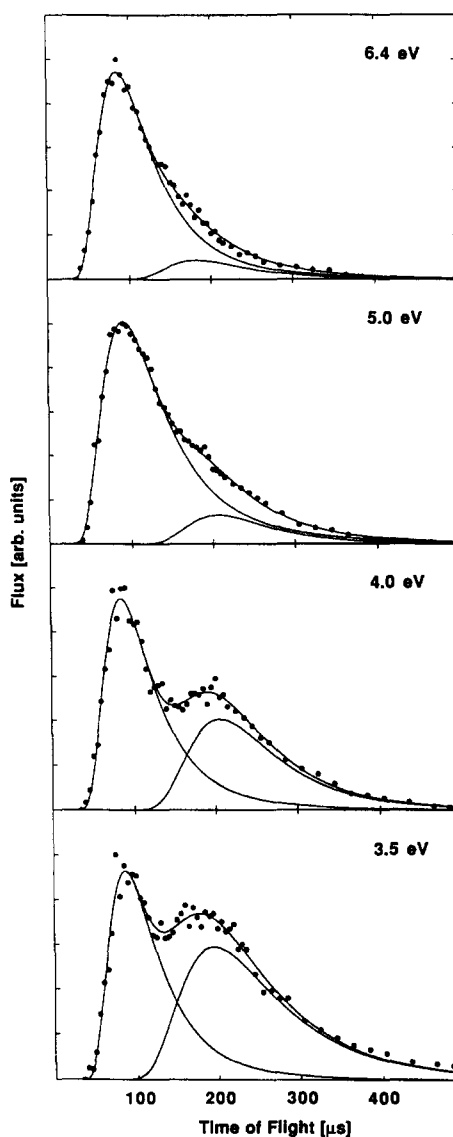
FIG. 7. Time-of-flight spectra obtained with the mass spectrometer. Shown are the data converted to flux. The photon energies used to initiate the desorption are 6.4, 5.0, 4.0, and 3.5 eV from the top to the bottom panel, respectively. The lines represent least-squares fits using a superposition of two modified Maxwell–Boltzmann distributions. The spectra are vertically not at scale; in fact the bottom spectra, e.g., is enlarged by a factor of approximately 20.
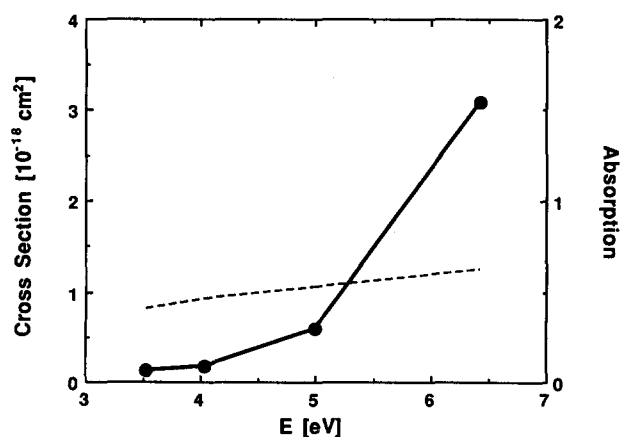

FIG. 6. Photodesorption cross section as function of photon energy as obtained based on the data shown in Fig. 5. The dashed line gives the absorption coefficient of palladium.

C. Integral time-of-flight spectra

Using the quadrupole mass spectrometer to detect the desorbing molecules, the first finding is that at 6.4 eV excitation energy at least 90% of the released molecules are NO. Based on the signals observed at 46 amu only a small contribution from NO$_2$ is found. There was no indication for any other desorbing species.

Time-of-flight spectra have been obtained using a geometry at which the laser beam is incident perpendicular to the surface and the QMS is placed at an angle of 25° with respect to the crystal normal. The TOF data depicted in Fig. 7 have been converted to flux so that the area under a given portion of the curve is directly proportional to the number of molecules released.

Generally, bimodal velocity distributions are recorded. This is most obvious in the lowest panel which reproduces the data obtained at 3.5 eV. The data has been fit by a superposition of two modified Maxwell–Boltzmann distributions [Eq. (1)] in order to extract the mean translational energy $\langle E_{\mathrm{trans}} \rangle$ and the relative population in the two contributions observe. For the fast contribution we obtain $\langle E_{\mathrm{trans}} \rangle / 2k = 70$ meV. This would correspond to a surface temperature of 800 K, which is far above the maximum substrate temperature reached. For the slow channel we derive a value of 135 K (11 meV). This value is close to the calculated maximum temperature (120 K) of the crystal during the laser pulse.

The partitioning of the desorbing molecules into the two channels is markedly dependent on the excitation energy. With increasing photon energy the relative weight of the fast contribution rises rapidly. At 6.4 eV the slow channel is no longer obvious in the raw data, but for reasons of consistency, we include it in the fit, attributing the same mean velocity to it as we obtained in the other fits.

Most striking is the fact that the position of the TOF maximum of the fast channel does not change with the variation of excitation energy. The obtained values for the position of the peak and $\langle E_{\mathrm{trans}} \rangle$ are constant within an error range of 10%. Although the photon energy offered to the adsorbate/substrate complex differs by a factor of 2, only a constant amount is finally converted into translational energy of the ejected NO molecule. Less striking perhaps, but still worth noting, is that the parameters describing the position and width of the slow channel are also independent of wavelength.

By combining the data obtained from the cross section measurements, Fig. 5, and the integrated areas of the two channels in the time-of-flight spectra, we can estimate the partial cross sections. Due to the fact that the TOF spectra were recorded at a single fixed angle, this procedure is, however, only applicable if we assume that the angular distributions, which might be different for the two channels, do not vary significantly with photon energy. In this case we can separate the energetic and the angular part and assume the angular function to be independent of photon energy. The exact ratio of the partial cross sections is then still unknown, but their variation with wavelength can be derived in this way.

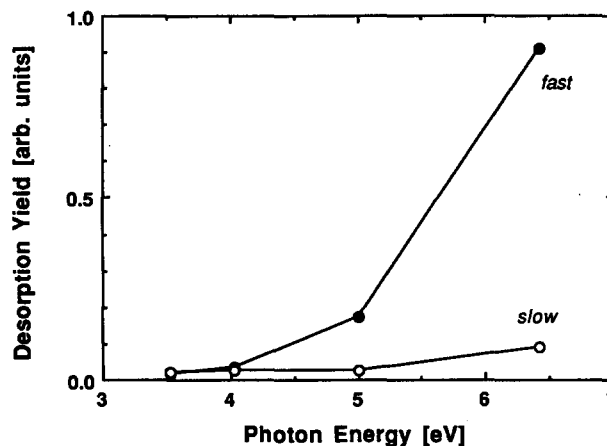It now turns out that the yield in the slow channel varies

FIG. 8. Partial yields for the fast and slow channel vs photon energy (●: fast channel; O: slow channel).

only little with photon energy (Fig. 8). It is the fast channel which is responsible for the rapid increase of the cross section above 4 eV photon energy.

The data have to be interpreted in a way that two desorption channels are present, but in both cases the NO has first to be produced by photodissociation. In the following we will therefore classify the two contributions as "slow channel" and "fast channel."

D. State specific data for 6.4 eV excitation

Using LIF detection of the desorbing molecules allows us to study in detail the channeling of energy into the various degrees of freedom. Two different approaches are possible and lead to sets of complimentary data. First, the time delay between the desorption and probe lasers is kept fixed. By scanning the wavelength of the probe laser, the rotational state distribution of the molecules is tested for a fixed velocity. Alternatively, the probe laser is tuned to a fixed molecular transition and scanning the time delay between the two lasers provides a TOF spectrum for a single rovibronic state of the desorbed molecules. The data to be presented refer always to 193 nm (6.4 eV) excitation.

Figure 9 gives three examples of TOF spectra for different rotational levels of the vibrational ground state ($v = 0$). The data has been obtained using transitions of the R_{11} branch in all cases. Again, we find bimodal velocity distributions. At low J the slow channel is predominant. With increasing rotational excitation the fast channels gains weight. It is also noteworthy that the position of the fast channel shifts to shorter times for higher J. Similar TOF spectra have been taken up to $J = 34.5$ for both fine structure states of the NO($X\,^2\Pi$) doublet.

Using the same fitting procedure as for the integral data, we have extracted mean translational energies for the fast channel (Fig. 10). A linear increase of the kinetic energy with internal energy is observed starting from 680 K for low J and reaching 1900 K for $J = 3.45$. The values derived for the two fine-structure states do not differ systematically when the sum of rotational and fine-structure energy is used to define the internal energy.
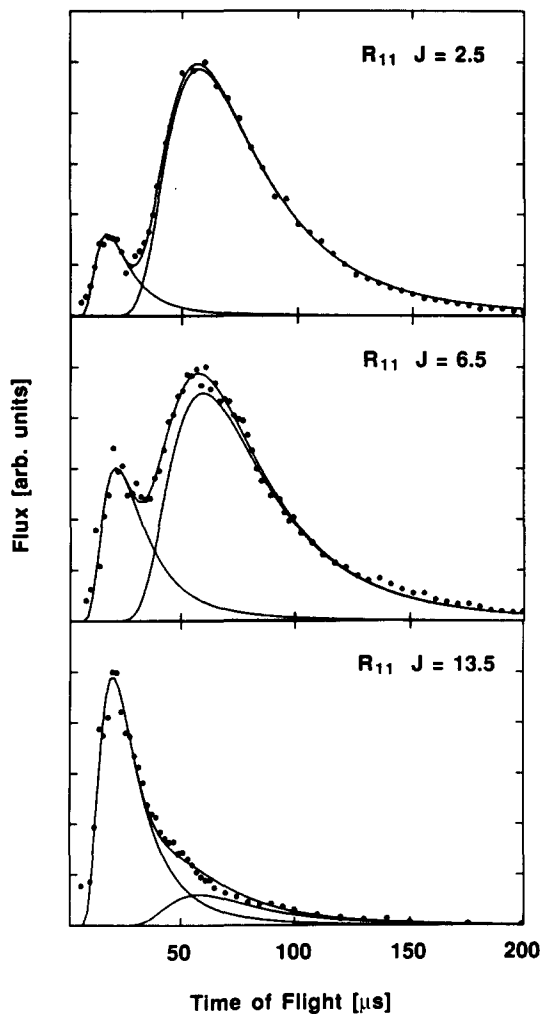
FIG. 9. State resolved time-of-flight spectra for three different rotational levels of desorbed NO molecules (top: $J = 2.5$; middle: $J = 6.5$; bottom: $J = 13.5$). The lines represent least square fits using two modified Maxwell–Boltzmann distributions.

FIG. 11. Mean translational energy vs rotational energy of NO desorbed in the slow channel for 193 nm excitation. (O: $^2\Pi_{1/2}$; ●: $^2\Pi_{3/2}$).

The equivalent data for the slow channel are shown in Fig. 11. Here mean translational energies scattering around 140 K are obtained which are—within the experimental uncertainties—independent of the internal energy. For higher rotational levels the slow channel—although still clearly present—becomes so ill defined in the noise of the tail of the fast channel that the fitting procedure is no longer able to extract reliable mean energies.

Rotational state distributions were obtained for several fixed flight times. At a delay corresponding to a velocity of 1100 m/s the data depicted in Fig. 12 has been obtained. In the Boltzmann graph all points obtained at various transitions belonging to different branches of the NO $\gamma(0,0)$ band are adequately represented by a single line yielding a rotational temperature—a measure of the average rotational excitation—of 900 K. At velocities of 1470 m/s and 890 m/s, we obtain rotational temperatures of 1050 and 710 K, respectively. When we finally try to model the TOF spectra
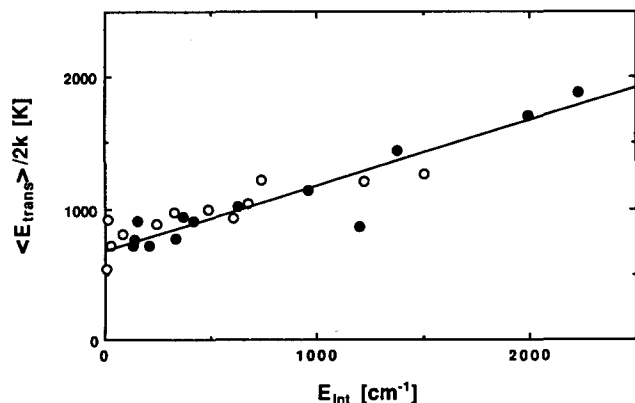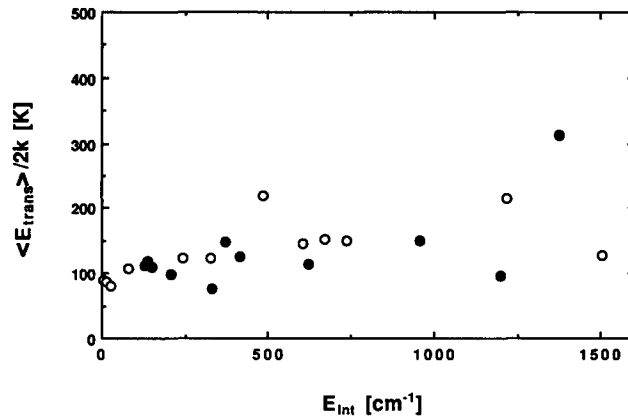

FIG. 10. Mean translational energy vs rotational energy of NO desorbed in the fast channel for 193 nm excitation. The line gives a linear fit to the observed correlation of both energies. (O: $^2\Pi_{1/2}$; ●: $^2\Pi_{3/2}$).
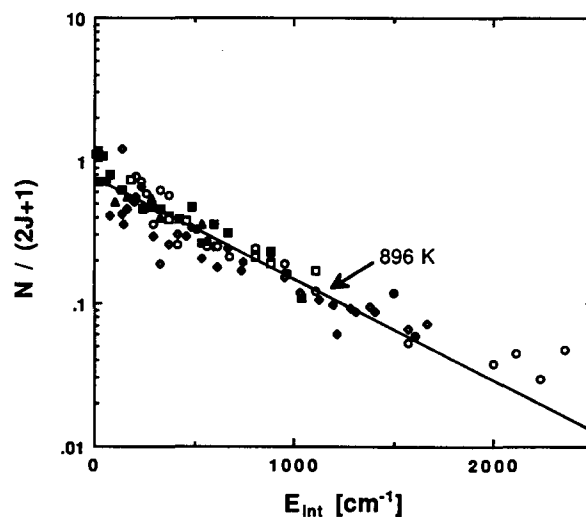

FIG. 12. Boltzmann plot of the rotational distribution for NO desorbed in $v = 0$ in the fast channel (velocity: 1100 m/s). The various symbols indicate different branches of the NO $\gamma(0,0)$ band. The closed and open symbols belonging to the $^2\Pi_{1/2}$ and $^2\Pi_{3/2}$ manifold, respectively. The line gives a linear fit yielding a rotational temperature of 896 K.

based on the mean translational and rotational energies derived from our experiments it turns out that the assumption of 900 K for the rotational temperature of the fast channel is a good representation. We therefore conclude that this value describes best the whole ensemble of the fast channel.

The rotational state distribution of the slow channel— obtained at a delay setting corresonding to a velocity of 250 m/s—cannot be represented by a single line in a Boltzmann plot (Fig. 13). Instead we find two regions. Up to internal energies of 250 cm^{-1} ($J \leqslant 11.5$ in the $^2\Pi_{1/2}$ state) the distribution falls off rapidly, corresponding to a temperature of 115 K. For higher internal energies a contribution is found which evolves with a rotational temperature of 470 K. The whole slow channel can be regarded as a superposition of two contributions, one being rotationally cold and having a weight of 90% and one being more excited which carries the remaining 10%. The flux ratio for individual lines is then given by the Boltzmann factors times the 9:1 ratio. We carefully checked that reflections from parts of the apparatus or residual background did not give rise to this unexpected contribution. We note that it is also seen in the TOF spectra and it changes, as expected, its position in time, when the distance between crystal and detection volume is varied.

Signal levels in the first vibrationally excited state, $v = 1$, were too low to allow a detailed study. But from the observation of some lines of the $\gamma(1,1)$ band which overlaps with high J transitions of the $\gamma(0,0)$ band we conclude that the population in $v = 1$ is of the order of a few percent. It should be pointed out that we only tested low J of the $v = 1$ population and the overall rotational distribution in $v = 1$ may differ very strongly from that observed in $v = 0$. Nevertheless, this finding of a vibrationally excited population of a few percent indicates a vibrational temperature in excess of 1000 K. No information has been obtained about possible desorption in even higher vibrational states.

E. Changes with surface temperature

We also found an interesting variation of TOF spectra with changing substrate temperature (Fig. 14). The experiments were carried out using the QMS for detection and the ArF laser light (6.4 eV) for excitation. For base temperatures of 95 to 115 K the signal in the fast channel changes only slightly. This signal, and also the total yield, shows a rapid fall off when the crystal temperature approaches 135 K. This is readily explained by the fact that at this temperature thermal desorption of NO₂ starts. Therefore, the coverage present during the laser pulse is determined by the fraction of molecules which do not desorb thermally in the interval between the gas pulse and firing the laser, because in this temperature range, incoming NO₂ molecules from the nozzle pulse will undergo a trapping/desorption process. Above 150 K, no more signal is detectable in either the slow or fast channel.

A striking feature is that, with increasing temperature, the intensity of the slow channel increases with respect to the fast one (Fig. 14). It seems reasonable, based on Fig. 3, to
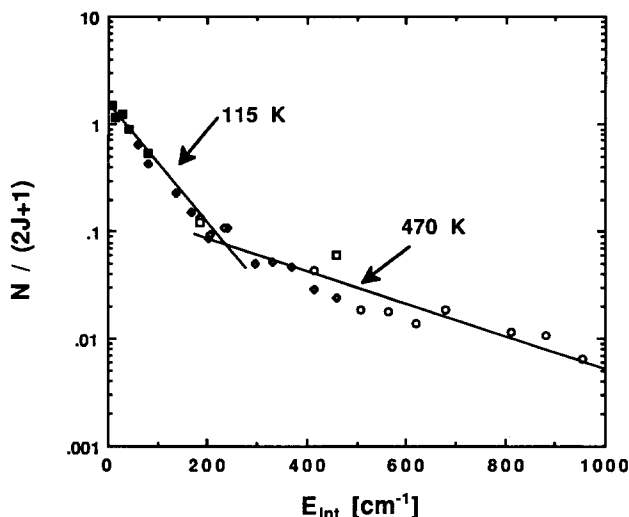

FIG. 13. Boltzmann plot of the rotational distribution for NO desorbed in the slow channel (velocity: 250 m/s). The data can only be fitted in two separate regimes by rotational temperatures of 115 and 470 K for low and high internal energies, respectively. For explanation of symbols used see Fig. 12.
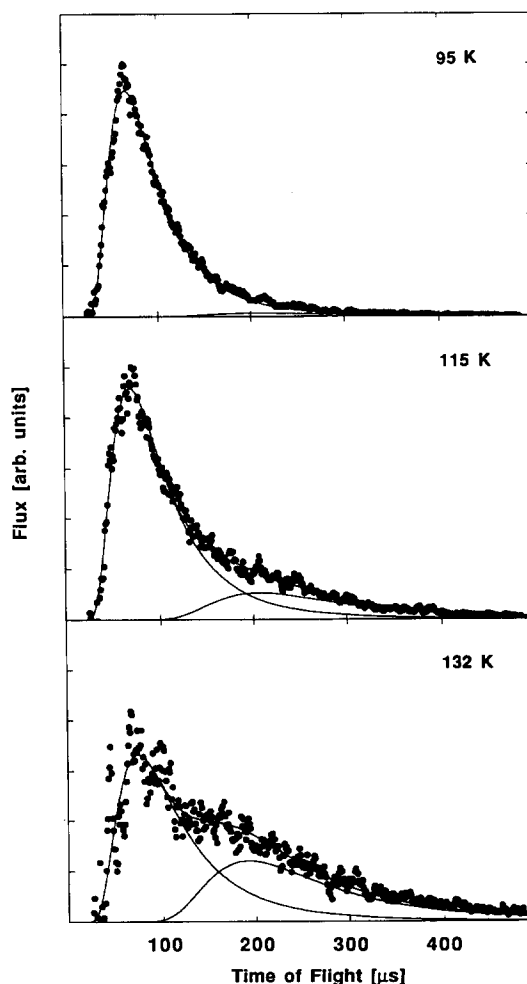

FIG. 14. Time-of-flight spectra for NO desorbed at different crystal base temperatures using 193 nm radiation. A strong decrease of the yield in the fast channel is observed corresponding to a reduced steady state coverage at this temperatures. Relatively the slow channel shows a strong increase in yield. Top: 95 K; middle: 115 K; bottom: 132 K.
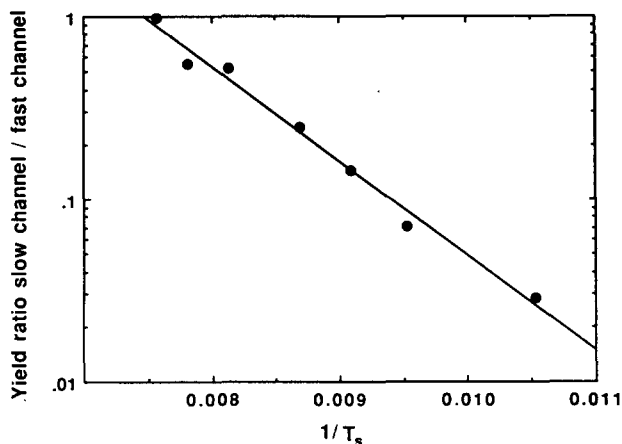
FIG. 15. Arrhenius plot of the yield in the slow channel. The intensity in the slow channel has been normalized to the decrease of coverage by division through the signal in the fast channel. The fit indicates an activation energy of 100 meV.
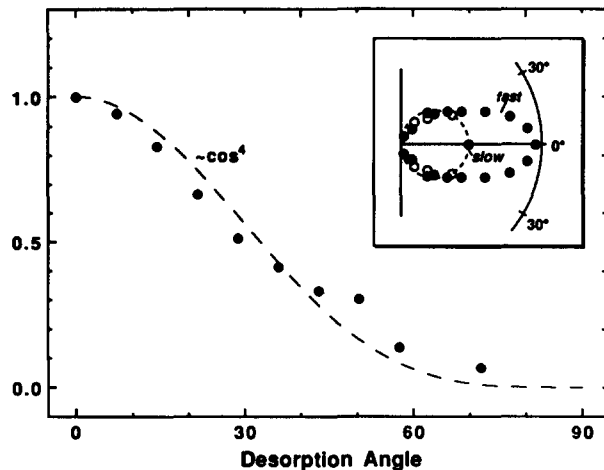

FIG. 16. Angular distribution of the desorption flux in the fast channel. The solid curve gives a cos^4 fit to the data, which is found to represent the data best. The inset shows the same data in a polar plot. Also shown is the data for the slow channel, which is well represented by a cosine distribution.

assume that the intensity in the fast channel is a measure of the available coverage at each temperature. We can, therefore, take the ratio of the signals in the slow and fast channels and consider it as the yield of the slow channel normalized with respect to the coverage n_s. Figure 15 presents the data in the form of an Arrhenius plot, log n_s vs $1/T_s$. From the slope we derive an activation energy of 100 meV, which is only a third of the condensation energy of NO_2. The obtained value is in much better agreement with the heat of vaporization of NO (≈ 0.15 eV).[33] This might well indicate that the slow channel already desorbs with the characteristics of thermal desorption of physisorbed NO.

F. Angular distribution

The angular distribution of the desorbing flux has been measured using mass spectroscopic detection and 6.4 eV excitation. In order to allow to position the QMS close to the surface normal the laser has been directed onto the crystal 23° off the normal direction. For each angle a TOF spectrum has been recorded using the signal obtained during the first shots. Evaluation of these yields the angular distribution of the slow and the fast component separately. The positions of both contributions show no displacement in flight time when the angle is varied. The fast channel shows an angular distribution which is sharply peaked in forward direction (Fig. 16), whereas the slow channel is well described by a cosine distribution. The angular distribution of the fast channel is best described by a cosine to the fourth curve.

The same distribution has been found for a wide range of initial NO_2 coverages (0.1–0.4 ML). For higher, multilayer coverages the angular distribution is ever sharper peaked in the normal direction. The laser fluence has been varied in order to eliminate concerns that the peaking in normal direction is caused by collision between the desorbing molecules establishing a nozzle expansion like behavior. Between 7 and 1.2 mJ/cm^2 fluence no variation of the angular distribution is observed.

G. Polarization probe of primary excitation mechanism

Utilization of the transverse polarized nature of light has proven to be of great assistance in many investigations of problems in molecular and surface physics. As an example, we need only to mention the use of polarized radiation in studies of photoelectron spectroscopy of adsorbates and their importance for the elucidation of adsorbate geometries.[34] Up to this point, we have exclusively presented experiments carried out using normal incidence of the excitation light. This radiation was unpolarized and had electric field components solely in the plane of the metal surface.

In the following, we present an experiment using polarized radiation. By examining the polarization-dependent desorption yield, as a function of angle of incidence, we demonstrate that absorption by the metal, rather than direct absorption by the adsorbate, is the dominant mechanism for the photochemical process studied.

Ellipsometric experiments have revealed that the macroscopic Maxwell equations provide an adequate description of the electromagnetic field close to an interface,[35] which may then be considered to interact with the adsorbate.

Figure 17 sketches the geometry at the plane boundary between vacuum and the metal surface. Because our experiments, in general, were carried out at less than 1 ML coverage, we will neglect the refractive properties of this very thin overlayer, which are unknown. The electric field description is then governed by one material property, the complex index of refraction of the metal n_2 ($\mu = 1$), which depends on photon energy.

Part of the incident light is reflected at the interface, the rest is refracted into the substrate and absorbed within a penetration depth of about a tenth of the wavelength. The incident light can be subdivided into two independent polarizations, one with the electric field vector parallel to the plane of incidence (p polarization) and the other perpendicular to it (s polarization).
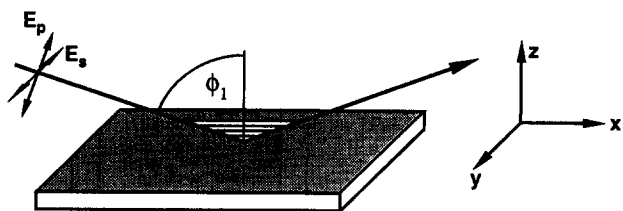
FIG. 17. Schematic drawing of the optical geometry at the metal interface: the light beam has two principle polarizations. One perpendicular and one parallel to the plane of incidence. At the interface three components of the electric field are to be considered. They are named according to the coordinate system shown at the right.

FIG. 18. Desorption yield as function of the angle of incidence for excitation with light being polarized parallel (p: ■) and perpendicular (s: □) to the plane of incidence. The curves give the absorption in the metal substrate (—) and the electric field intensities at the interface (– –). The absorption differs for both cases of polarization. In the case of s polarization the field intensity has only a component in the plane of the surface $\langle E_{s,y}^2\rangle$, in the case of p polarization two components one in the surface plane $\langle E_{p,x}^2\rangle$ and one normal to it $\langle E_{p,z}^2\rangle$ are to be considered.

The incoming and the reflected waves form a standing wave at the boundary. In the case of an absorbing material, this wave stretches into the bulk. For s polarization only a component parallel to the surface $\langle E_{s,y}^2\rangle$ can exist. For p polarization two components are present: one in the plane of the surface $\langle E_{p,x}^2\rangle$ and one parallel to the surface normal $\langle E_{p,z}^2\rangle$.

We now briefly summarize the results of the electromagnetic theory as presented, for example, by McIntyre.[36] The Fresnel coefficients correlate the electric field amplitudes of incident and reflected light

$$r_s = \frac{\cos\phi_1 - \sqrt{n_2^2 - \sin^2\phi_1}}{\cos\phi_1 + \sqrt{n_2^2 - \sin^2\phi_1}}, \quad (3)$$

$$r_p = \frac{n_2^2\cos\phi_1 - \sqrt{n_2^2 - \sin^2\phi_1}}{n_2^2\cos\phi_1 + \sqrt{n_2^2 - \sin^2\phi_1}}, \quad (4)$$

where ϕ_1 is the angle of incidence. The reflectivity at the boundary is then given by

$$R_i = |r_i|^2 = r_i \cdot r_i^*, \quad (5)$$

where the subscript stands for the two polarization cases. The absorption coefficients are then calculated by

$$A_i = 1 - R_i. \quad (6)$$

From the Fresnel coefficients, we can also derive the absolute phase changes upon reflection for the two polarizations. They are given by the quantities δ_s and δ_p with

$$\delta_i = \tan^{-1}\left[\frac{\mathrm{Im}(r_i)}{\mathrm{Re}(r_i)}\right]. \quad (7)$$

The mean-square electric field strength of the different components in the standing wave at the boundary is then given by—assuming unity amplitude of the incident wave—

$$\langle E_{s,y}^2\rangle = (1 + R_s) + 2\sqrt{R_s}\cos\delta_s,$$

$$\langle E_{p,x}^2\rangle = \cos^2\phi_1\{(1 + R_p) - 2\sqrt{R_p}\cos\delta_p\},$$

$$\langle E_{p,z}^2\rangle = \sin^2\phi_1\{(1 + R_p) + 2\sqrt{R_p}\cos\delta_p\}. \quad (8)$$

With this set of equations all relevant quantities can be easily calculated based on the optical constants for Pd.[37] Figure 18 shows the electric field intensities and absorption coefficients as function of angle of incidence for 193 nm radiation. F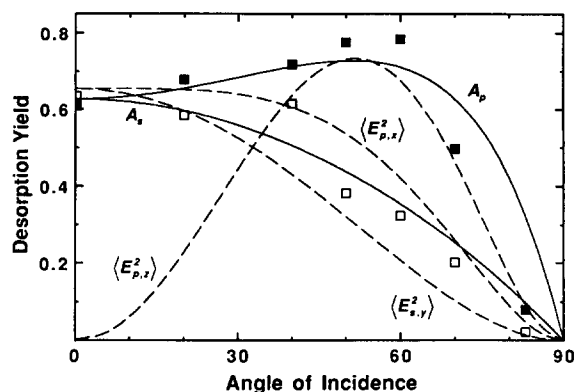or perpendicular incidence, the absorption is independent of the polarization. With increasing angle of incidence the absorption for the p component passes through a maximum, whereas the absorption for the s component decreases continuously. At grazing incidence no light will be absorbed.

The field intensity of the component parallel to the metal surface decreases, for both polarization cases, monotonically to zero. But the field component parallel to the surface normal $\langle E_{p,z}^2\rangle$ is zero at normal incidence, shows a pronounced maximum, and falls then to zero at large angles.

The absorption by an adsorbate A_{mol} will be dependent on its molecular orientation determining the direction of the transition dipole moment μ with respect to the total electric field vector **E** at the surface

$$A_{mol} \approx (\mathbf{E}\cdot\mu)^2. \quad (9)$$

If, for example, a molecule is oriented with its axis normal to the surface and exhibits a perpendicular transition dipole moment, only the field components parallel to the surface will contribute to the absorption by the molecule. In the opposite case, a molecule with a transition dipole moment along the surface normal, only the z component in the case of p polarization can be absorbed by the molecule and there will be no absorption for s polarization. In the most general case for p polarization, both components can contribute, but they are weighted by the cosine squared of their respective angle to the direction of μ.

We measured carefully the desorption yield as function of angle of incidence, switching between s and p polarization at each angle. The angle was changed in a nonmonotonic manner. The QMS used for detection was kept at a fixed angle ($23.5°$) with respect to the surface normal in order not to change the detection geometry. The initial yields, starting from a well-defined coverage, were corrected for the cosine dependence of the laser fluence through the crystal surface with varying angle. Data evaluation is possible in two ways: First, we compare the individual data points with the calcu-

lated curves (Fig. 18). Second, we take the ratio between the yields at each angle (Fig. 19). This procedure removes much off the scatter induced by systematic experimental errors due to the changing geometrical arrangement and instrument variations over time.

In Fig. 18 the whole set of data points has been scaled to match the calculated curves at normal incidence. As can be seen, a substantial amount of scatter is still present. But it is clearly evident that the data for *p* polarization show a maximum at intermediate angles and do not fall off at smaller angles as the data points for *s* polarization do. This is nicely fit by the curves for absorption in the metal.

In order to fit the data with the direct absorption model we are forced to assume, because of the nonzero signal for *p* polarization and because of the maximum in the *p* polarization yield, that not only a field component within the surface, but also a contribution in the direction of the surface normal is active. To fit the data we have to combine one third of $\langle E_{p,z}^2 \rangle$ with $\langle E_{p,x}^2 \rangle$. In that case a curve results which approaches closely the curve for absorption in the metal.

Thus we have an ambiguity, and, in order to eliminate it, we have examined the measured *ratios*. We find that the experimental data is well represented by the calculated ratios for metal absorpton, but not by the direct absorption model, in the two polarization cases. Calculating the ratio, based on the above fit to direct absorption, using

$$\frac{\langle E_{p,x}^2 \rangle + \frac{1}{3}\langle E_{p,z}^2 \rangle}{\langle E_{s,y}^2 \rangle}, \tag{10}$$

predicts values which are clearly too large at inclined angles of incidence. Because these ratios remove much of the systematic experimental error, and are therefore more reliable, this is considered as clear evidence for the invalidity of the direct absorption model.

We could also argue the other way around starting with the measured ratios. The ratio between the field components in the surface for *s* and *p* polarization ($\langle E_{p,x}^2 \rangle / \langle E_{s,y}^2 \rangle$) is practically identical to the ratio for absorption (A_p/A_s).
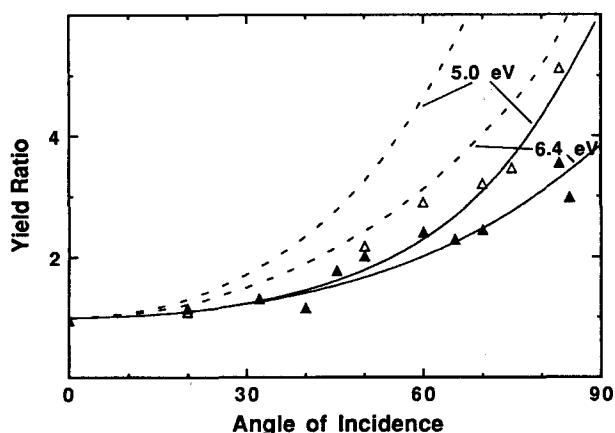

FIG. 19. Ratio of the observed yields as function of the angle of incidence (▲: 6.4 eV; △: 5.0 eV). The solid lines give the prediction from theory when assuming that absorption in the metal is the initial step in the photodissociation/desorption process. The dashed curves come from a model of direct absorption by the adsorbate.

Therefore taking only them into account would fit the experimental ratios. We would then be forced to assume that the field component normal to the surface does not contribute, i.e., that the transition dipole moment would be in the plane of the boundary. But this can be ruled out because the individual data sets do not fit the theoretical curves (Fig. 18). Namely, the data for *p* polarization is not fit by the $\langle E_{p,x}^2 \rangle$ curve alone because the latter does not show a maximum at $\sim 60°$.

Quite similar conclusions were reached for 5.0 as well as 6.4 eV photon energies, as also depicted in Fig. 19.

We propose the method presented here as a way to determine the dominant mode of absorption in an adsorbate/substrate system. In our case, we find that the data is best explained by assuming that absorption in the metal is the dominant primary step in the photochemical process under study.

IV. DISCUSSION

A. Evidence for surface photochemistry

Adsorption of NO_2 on the Pd(111) surface precovered with NO up to saturation leads to the continuous growth of a single desorption peak in TPD. This indicates the occurrence of condensation on an inert substrate surface. At the temperatures applied (≈ 100 K) this process will be accompanied by dimerization and the build-up of solid N_2O_4. The desorption energy estimated from the temperature of the TPD peak is of the same order as the heat of sublimation of N_2O_4 (0.45 eV).[38] This is also in agreement with the conclusion reached for NO_2 multilayers on Pt(111)[31] and Ru(001)[39]; in the latter case the vibrational frequencies were found to be very similar to those of gaseous N_2O_4. This molecule has a planar structure (D_{2h} symmetry), the O–N bond length and the O–N–O bond angle are nearly identical to those of the free NO_2 ($\tilde{X}^2A_1$: $R_{ON} = 1.19$ Å, $\angle_{ONO} = 134.5°$).[40] The dimerization energy (0.54 eV) is much smaller than the energy necessary for the dissociation step $NO_2 \rightarrow NO + O$ (3.11 eV). The TPD peak at 140 K has to originate from N_2O_4, while further thermal decomposition into NO requires even higher temperatures. Hence, also the NO molecules observed as a consequence of UV irradiation have to be of *nonthermal origin*.

One might still consider the possibility that this species originates from thermally desorbed N_2O_4 (or NO_2) which is subsequently photodissociated in the gas phase by the laser light used for desorption. This may be ruled out because of several considerations:

The cross sections for gas phas absorption—even though they are rather large—are at least two orders of magnitude too small to completely dissociate all molecules desorbed. Therefore a overwhelming background of NO_2 would be expected, which is not found.

At the low laser fluences used, a temperature jump of less than 20 K is expected. Due to the fast heating rate the maximum desorption yield would occur at much higher temperatures than in conventional thermal desorption spectroscopy. Because of the transient character of the temperature jump (≈ 100 ns) only a negligible fraction will desorb during this time. And secondly the surface reaches the peak

temperature as late as the tail of the laser pulse. Therefore most molecules would desorb thermally at times when the laser intensity is already declining. Consequently, the probability for photodissociation would be even smaller than estimated above.

The NO state distributions do not resemble those known for gas phase photodissociation of NO_2 or N_2O_4. N_2O_4 photolysis leads predominantly to NO_2, and not to NO. Photodissociation of gaseous NO_2, on the other hand, yields rotational (and vibrational) state distributions of NO which are completely different from those observed here. Similarly, the TOF spectra and their dependence on photon energy, as well as the absence of an O signal in the mass spectrum, cannot be reconciled with a gas phase photolysis process.

It is therefore without doubt that *the NO molecules observed originate from photolysis of the N_2O_4 adlayer.*

B. Mechanism

The experiments performed with polarized radiation at varying angles of incidence have clearly shown that the observed photodissociation yields can only be reconciled with a mechanism based on primary light absorption in the Pd metal, but not by adsorbed molecules—whatever orientation on the surface they would have.

For $h\nu \gtrsim 4$ eV the cross section for photodissociation of adsorbed NO_2 is considerably larger than for the free molecules. Gaseous N_2O_4—albeit exhibiting higher absorption coefficients—is split by photons into 2 NO_2,[19] so that the absorption cross section for NO_2 is governing the formation of NO. Since additional channels for relaxation of the excitation energy exist at a surface, the cross section for photodissociation would necessarily be smaller than in the free molecule if it would be determined by absorption in the molecule itself. (Since the interactions of N_2O_4 in the adsorbed layer are rather weak any marked variation of the UV absorption coefficients due to molecular distortions may certainly be ruled out.) The observed photodissociation cross section can, on the other hand, be easily reconciled with a mechanism based on light absorption by the metallic substrate as the primary step: At $h\nu = 6.4$ eV, for example, a densely packed monolayer of NO_2 ($\approx 1.0 \times 10^{15}$ molecules/cm^2) would absorb only a fraction of about 3×10^{-4} of the incident radiation, while about 63% are absorbed by the Pd substrate in a depth of about 40 Å. If all of these electronic excitations would *survive* and subsequently transform into valence electronic excitation of the NO_2 molecules (leading to dissociation) then the cross section for photodissociation of adsorbed NO_2 would exceed that of free NO_2 by a factor of 2000, while actually a factor of 10 is observed. This estimate demonstrates, on the other hand, that with the present system an efficiency for bond breaking within adsorbed molecules initiated by electronic excitation of a metallic substrate of the order of one percent can be reached.

The clean Pd(111) surface has a work function of 5.6 eV.[41] Whereas unsaturated layers of NO change the work function, it turns out that the saturated layer of NO reestablishes the original value.[29] Hence 6.4 eV photons will excite electrons from the Fermi level to above the vacuum level

(photoelectrons), while with $h\nu = 5.0$ eV hot electrons are created which may penetrate the potential barrier at the metal/adsorbate interface through tunneling. Inside the metal the mean free path of these electrons will be very large, because of their very small kinetic energy, so that even electrons excited deeper in the bulk will reach the surface with fairly high probability. Therefore it appears that both kinds of electrons excite the adsorbed N_2O_4 finally into the same state from which it fragments. The energy distribution of the hot electrons generated will depend on the band structure of Pd(111) and the excitation energy. The ease by which the potential barrier at the interface may be crossed will, on the other hand, increase with electron energy. From gas phase work it is known that electron attachment cross sections show sharp resonances which coincide with ionic states.[42] Therefore it is expected that the adsorbed N_2O_4 picks up only electrons of a specific energy range. This may offer a plausible explanation for the observed resonance like variation of the cross section.

Once the electronic excitation has passed the interface the chemisorbed NO overlayer forms obviously a rather efficient inhibitor for quenching. In other words, since the N_2O_4 molecules adsorbed on top of the NO layer are only weakly coupled, to the metallic substrate, the latter will be inefficient for electronic relaxation, and the dissociation probability is high as soon as the electronic excitation has reached the N_2O_4 molecules. If, on the other hand, NO_2 is directly chemisorbed on the Pd surface, the photodissociation cross section is observed to be reduced by at least two orders of magnitudes. This is in qualitative agreement with data reported for photodesorption: Photodesorption of NO from nonmetallic surfaces such as NiO or Si was suggested to be mediated by hot electrons and occurs with high cross sections, while for NO/Pt(111) only a very small value of the order of 10^{-22} cm^2 was evaluated.[11] This conclusion is further in agreement with general experience from electron stimulated desorption (ESD) studies.[43]

The elementary step leading to splitting of the NO_2 can most probably be classified as dissociative electron attachment process, i.e., bond breaking initiated by the transient formation of a negative ion,

$$e^- + AB \rightarrow AB^- \longrightarrow A + B^-$$
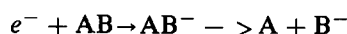
whereby B^- will subsequently release its negative charge (from the ground state) back to the metallic substrate. A mechanism of this type has, for example, been suggested for the photofragmentation of CH_3Cl on Ni(111).[8] More specifically, in the present case the particular electronic structure of condensed N_2O_4 has to be considered. Although bulk condensation at 80 K was found to lead to the predominant formation of symmetric (D_{2h}) $O_2N–N–NO_2$ dimer, it was observed that upon increasing the temperature spontaneous transformation into the ionic form $[NO]^+[ONO_2]^-$ (with distinctly different vibrational spectroscopic features) takes place.[44] The existence of this "nitrosonium nitrate" species reflects the ease of electronic and atomic redistribution processes in solid N_2O_4. Free NO_2 has an electron affinity of 2.27 eV,[45] while the value for N_2O_4 is unknown. The reaction $e^- + N_2O_4 \rightarrow NO + NO_3^-$ is exothermic by 2.6 eV.[46] Hence

with an effective work function of 5.6 eV, a minimum photon energy of about 3.0 eV would be required in order to excite a metal electron from the Fermi level to the necessary energy level. This conclusion can at least qualitatively be reconciled with the experimental findings.

We may now speculate that this latter process can be triggered by electron attachment in the adsorbed layer. In view of the tendency to form $NO^+NO_3^-$ this might be considered as neutralization of the NO^+ by electron capture. Regardless of the initial energies of the hot electrons this latter process would start from the same initial state, and this would explain why the mean translational energy of the desorbing NO is independent of the primary excitation energy. The nonthermal energy distributions of the fast molecules demonstrate, on the other hand, their origin from the repulsive part of an interaction potential. There will, however, also be a finite probability for thermal accommodation at the surface preceding to desorption, leading to the slow channel with energy distributions corresponding to the surface temperature. In view of the small physisorption energy of NO (≈ 0.15 eV)[33] the mean surface residence time of this species will, even at 100 K, be still much shorter[47] than the flight time so that again desorption may be regarded as "instantaneous."

There exists still another fundamental difference between photodissociation processes of free molecules and in the condensed state. In the former case the fragments will separate from each other essentially without further collision, while in a system like the present one there is a much higher probability for mutual encounters. More specifically, the initial pair of fragments may recombine again–an effect which has been known for photodissociation reactions in liquid phase for many years (geminate recombination)[48] and where its efficiency has been found to depend on density and temperature, etc. With the present system, clearly those particles which accommodate with the surface (the slow channel) will have longer residence times on the surface. This might well be the reason for the increase of the relative proportion of slow molecules with increasing temperature (Fig. 15): At higher temperature the trapped particles desorb more rapidly and hence there is a lower probability that they are lost by recombination. The apparent activation energy would be, the difference between the one for desorption and the one for migration, the latter being smaller. The slope resulting from Fig. 15 might then be interpreted as just this energy difference, which is certainly of the right order.

However, the mechanism for the formation of the NO molecules undergoing the trapping/desorption process is still unclear and it will need further experimental works to elude it. But the variation with excitation energy indicates that they might be of different origin than the fast channel.

The proposed mechanism would also offer an explanation for the apparent disappearance of the second reaction product, the O atoms. The NO_3^- species would be held to the surface through the image force, but the negative charge would rapidly tunnel back through the chemisorbed NO layer to the Fermi level of the metal. The tunneling probability would certainly be much smaller than that for the hot electron in the reverse process. The neutral NO_3 would be insta-

ble and expel either O or O_2. If its lifetime would, however, be of the order of 100 μs, the release of the oxygen species would be spread out so strongly on the time that its density would be below the detection limit of the QMS. It should be pointed out that never could any O species be detected on the surface in post-irradiation TPD if the surface was precovered with NO up to saturation. If this overlayer was incomplete, however, chemisorbed O atoms were found.[49]

C. Dynamics

In the following we focus on the dynamics of the photodissociation process giving rise to the fast channel. The distribution of energy over the various degrees of freedom of the fast NO molecules is distinctly different from the results reported for gas phase photolysis of NO_2. First of all, this difference will be due to the quite different electronic excitation and hence potentials from which bond breaking starts in both cases. Even more important, however, seems to be the vicinity of the metallic substrate. Only a small fraction of the excess energy offered by the adsorbed photon is carried away by the molecules leaving the surface. In fact, we find in the rotational and translational degrees of freedom only an average energy of ≈ 100 meV. This is in agreement with general experience also obtained with photodesorption[10] as well as with thermal dissociation of NO_2 on Ge[50] (where the excess energy originates from the reaction).

Since the present photodissociation reaction (as well as the effects of photodesorption and thermal dissociation mentioned above) may be considered as a process of half-collision[51] we may also adopt the basic idea of this concept, but we will have to incorporate the quenching of electronic excitations due to the proximity of the metal surface.

The minimum energy geometry of the unstable $N_2O_4^-$ is not known, but the geometry of NO_2^- ($R_{ON} = 1.25$ Å and $\angle_{ONO} = 117.5°$)[45] is very different from that of the NO_2 ground state. Because of the similarity of the ground-state geometry of the NO_2 monomer and its dimer, we are tempted to assume that negatively charged dimers will tend to put one of the NO_2 molecules in such a geometry, at least in an asymptotic limit. Therefore we can assume that as soon as the electron is attached to the adsorbate, energy will be transferred into motion of the nuclei resulting not only in dissociation but also in excitation of both, the bending motion and to some extent the stretching vibration.

This picture is consistent with the observed rotational states distribution and the observed extend of vibrational excitation. The excitation of the bending motion will cause a high extent of rotational excitation in the NO fragments. The difference in bond length between neutral and ionic NO_2 might cause the vibrational excitation.

We observe a positive linear correlation between rotational excitation and translational energy of ejected NO fragments: The mean translational energy *increases* with internal energy. The same has been seen for NO–NiO.[10] This can be explained based on the assumption of an excitation onto a repulsive potential surface on which the excitation is rapidly quenched by the metal. Only molecules which spend more than a critical time on this surface will gather enough kinetic energy to escape the ground-state potential well. It is the

time the individual molecules spend on the excited which determines the amount potential energy which is converted into kinetic energy. Asymptotically we will observe a distribution of kinetic energies which mirrors the distribution of life times in the excited. This is the well known Menzel–Gomer–Redhead picture.[52]

Adopting it for our case we have to consider at least two coordinates—the bending angle and the distance in the dissociation coordinate. Excitation from a ground to an upper state with differing geometries will cause motion in several coordinates including the bond that breaks. In the case of a rapidly quenched fragmentation process the amount of energy transferred into all degrees of freedom will be determined by the details of the potential surface *and* by the time the molecule stays on the excited potential energy surface. For that reason we would expect a positive correlation between the energies transferred to different degrees of freedom.

In our case we think that the repulsive potential energy curve is connected with the formation of a negative ion state. With respect to that state, the molecule is not in the minimum energy geometry. It will start to change its geometry and energy will be transferred into angular motion of the NO bonds and the stretch of the same bond distance. As soon as it is quenched back onto the ground-state energy surface, it will find itself in an energetically unfavorable geometry with respect to this surface. If the lifetime of the excitation has been long enough it might eventually fall apart releasing NO. The amount of rotational excitation and the translational energy will mirror the amount of energy transferred into the corresponding degrees of freedom away from the equilibrium geometry of N_2O_4.

Burns *et al.*[53] have argued with a similar model to explain their results for electron stimulated desorption of NO from Pt(111). Calculations based on this model produce translational and rotational energy distributions in qualitative agreement with their experimental findings. This concept seems therefore to be promising to explain results on a more quantitative basis than possible in the scope of this report. Classical trajectory calculations on a simplified model system reproduce the observed correlation between translational and rotational energies.[54]

ACKNOWLEDGMENTS

[1]T. J. Chuang, Surf. Sci. Rep. **3**, 1 (1983).
[2]S. R. Leone, Adv. Chem. Phys. **50**, 255 (1982); W. M. Jackson and H. Okabe, Adv. Photochem. **13**, 1 (1986); *Advances in Gas-Phase Photochemistry and Kinetics, Molecular Photodissociation Dynamics*, edited by N. M. R. Ashfold and J. E. Baggot (Royal Society of Chemistry, London, 1987).
[3]P. Avouris and R. E. Walkup, Annu. Rev. Phys. Chem. **40**, 173 (1989).
[4]Z. Ying and W. Ho, Phys. Rev. Lett. **60**, 57 (1988); W. Ho, Comments Cond. Mat. Phys. **13**, 293 (1988).
[5]E. B. D. Bourdon, J. P. Cowin, I. Harrison, J. C. Polanyi, J. Segner, C. D. Stanners, and P. A. Young, J. Phys. Chem. **88**, 6100 (1984); E. B. D. Bourdon, P. Das, I. Harrison, J. C. Polanyi, J. Segner, C. D. Stanners, R. J.

Williams, and P. A. Young, Faraday Discuss. Chem. Soc. **82**, 343 (1986); I. Harrison, J. C. Polanyi, and P. A. Young, J. Chem. Phys. **89**, 1475 (1988).
[6]F. L. Tabares, E. P. Marsh, G. A. Bach, and J. P. Cowin, J. Chem. Phys. **86**, 738 (1987).
[7]E. P. Marsh, M. R. Schneider, T. L. Gilton, F. L. Tabares, W. Meier, and J. P. Cowin, Phys. Rev. Lett. **60**, 2551 (1988).
[8]E. P. Marsh, T. L. Gilton, W. Meier, M. R. Schneider, and J. P. Cowin, Phys. Rev. Lett. **61**, 2725 (1988).
[9]S. A. Costello, B. Roop, Z. M. Liu, and J. M. White, J. Phys. Chem. **92**, 1019 (1988); Z.-M. Liu, S. A. Costello, B. Roop, S. R. Coon, S. Akhter, and J. M. White, *ibid.* (in press); B. Roop, K. G. Lloyd, S. A. Costello, A. Campion, and J. M. White, J. Chem. Phys. **91**, 5103 (1989); X.-Y. Zhu, S. R. Hatch, A. Campion, and J. M. White, *ibid.* **91**, 5011 (1989).
[10]F. Budde, A. V. Hamza, P. M. Ferm, G. Ertl, D. Weide, P. Andresen, and H.-J. Freund, Phys. Rev. Lett. **60**, 1518 (1988); P. M. Ferm, F. Budde, A. V. Hamza, S. Jakubith, G. Ertl, D. Weide, P. Andresen, and H.-J. Freund, Surf. Sci. **218**, 467 (1989).
[11]S. A. Buntin, L. J. Richter, R. R. Cavanagh, and D. S. King, Phys. Rev. Lett. **61**, 1321 (1988); L. J. Richter, S. A. Buntin, R. R. Cavanagh, and D. S. King, J. Chem. Phys. **89**, 5344 (1988).
[12]W. C. Natzle, D. Padowitz, and S. J. Sibener, J. Chem. Phys. **88**, 7975 (1988).
[13]A. M. Bass, A. E. L. Ledford, Jr., and A. H. Laufer, J. Res. Natl. Bur. Stand. Sect. A **80**, 143 (1976).
[14]C. H. Chen, D. W. Clark, M. G. Payne, and S. D. Kramer, Opt. Commun. **32**, 391 (1980).
[15]H. Zacharias, M. Geilhaupt, K. Meier, and K. H. Welge, J. Chem. Phys. **74**, 218 (1981); H. Zacharias, K. Meier, and K. H. Welge, in *Energy Storage and Redistribution in Molecules*, edited by Jürgen Hinze (Plenum, New York, 1983).
[16]T. G. Slanger, W. K. Bischel, and M. J. Dyer, J. Chem. Phys. **79**, 2231 (1983).
[17]R. J. S. Morrison and E. R. Grant, J. Chem. Phys. **77**, 5994 (1982); L. Bigio and E. R. Grant, J. Phys. Chem. **89**, 5855 (1985); J. Chem. Phys. **87**, 360 (1987).
[18]M.-R. Taherian, P. C. Cosby, and T. G. Slanger, J. Phys. Chem. **91**, 2304 (1987).
[19]M. Kawasaki, K. Kasatani, H. Sato, H. Shinohara, and N. Nishi, Chem. Phys. **78**, 65 (1983).
[20]K. Domen and T. J. Chuang, Phys. Rev. Lett. **59**, 1484 (1987).
[21]A. Mödl, H. Robota, J. Segner, W. Vielhaber, M. C. Lin, and G. Ertl, J. Chem. Phys. **83**, 4800 (1985).
[22]H. Conrad, G. Ertl, J. Küppers, and E. E. Latta, Surf. Sci. **65**, 235 (1977).
[23]D. Burgess, Jr., P. C. Stair, and E. Weitz, J. Vac. Sci. Technol. A **4**, 1362 (1986).
[24]*Physik Daten*, edited by H. Behrens and G. Ebel (Fachinformationszentrum, Karlsruhe, 1981), Vol. 18-1.
[25]This assumption has been made based on the voltages presented in the QMS. More accurate time-of-flight data is obtained using laser detection, where the time relation is better defined. The integral data has been compared to this measurement indicating a slightly higher flight time (~ 20 μs) through the QMS.
[26]M. S. Chou, A. M. Dean, and D. Stern, J. Chem. Phys. **78**, 5962 (1983).
[27]F. Budde, T. Gritsch, A. Mödl, T. J. Chuang, and G. Ertl, Surf. Sci. **178**, 798 (1986).
[28]H.-D. Schmick and H.-W. Wassmuth, Surf. Sci. **123**, 471 (1982).
[29]M. Bertolo and K. Jacobi, Surf. Sci. (in press); M. Bertolo, K. Jacobi, S. Nettesheim, M. Wolf, and E. Hasselbrink, Vacuum (in press).
[30]This data has been obtained using the mass spectrometer tuned on mass 30 (NO). NO_2 is detected on this e/m setting with a rel. probability of 60%.
[31]M. E. Bartram, R. G. Windham, and B. E. Koel, Surf. Sci. **184**, 57 (1987).
[32]This choice has been made because the structure of the physisorbed NO_2 layer is unknown. Some care has to be taken in order to avoid misleading results due the different pumping speeds observed for NO and NO_2. But at higher heating rates this effect becomes negligible. From the bulk density of N_2O_4 with 1.5 g/cm³ it is estimated that 0.5 ML are equivalent to one completed layer of NO_2.
[33]Landolt-Börnstein Band II, 4 Teil (Springer, Berlin, 1961).
[34]H.-J. Freund and M. Neumann, Appl. Phys. A **47**, 3 (1988).
[35]G. A. Bootsma and F. Meyer, Surf. Sci. **14**, 52 (1969).
[36]J. D. E. McIntyre, Adv. Electrochem. Electrochem. Eng. **9**, 68 (1973).
[37]We used as optical constants the following values: 5.0 eV; $n = 0.96$ and $k = 1.86$; 6.4 eV; $n = 0.73$ and $k = 1.29$, from Ref. 24.
[38]Gmelin, Bd. 4 (Verlag, Chemie, Berlin, 1936).

[39]U. Schwalke, J. E. Parmeter, and W. H. Weinberg, J. Chem. Phys. **84**, 4036 (1986).

[40]B. W. McClelland, G. Gundersen, and K. Hedberg, J. Chem. Phys. **56**, 4541 (1972).

[41]J. E. Demuth, Chem. Phys. Lett. **45**, 12 (1977).

[42]L. G. Christophorou, D. L. McCorkle, and A. A. Christodoulides, in *Electron–Molecule Interactions and Their Application*, edited by L. G. Christophorou (Academic, Orlando, FL, 1984), Vol. 1, pp. 478–617.

[43]D. Menzel, Nucl. Instrum. Methods B **13**, 507 (1986); in *Study of Surfaces and Interfaces by Electron Optical Techniques*, edited by A. Howie and U. Valdré (Plenum, New York, 1988).

[44]F. Bolduan, H. J. Jodl, and A. Loewenschuss, J. Chem. Phys. **80**, 1739 (1984).

[45]K. M. Erwin, J. Ho, and W. C. Lineberger, J. Phys. Chem. **92**, 5405 (1988).

[46]The heat of formation of NO₃⁻ is referenced as − 3.49 eV in: S. J. Ashcroft and G. Beech, *Inorganic Chemistry* (VanNostrand, London, 1973), p. 20.

[47]Assuming a frequency factor of 10^{13} s⁻¹ a residence time of 8 ns is calculated.

[48]A. L. Harris, J. K. Brown, and C. B. Harris, Annu. Rev. Phys. Chem. **39**, 341 (1988).

[49]M. Wolf, A. Cassuto, S. Nettesheim, E. Hasselbrink, and G. Ertl (to be published).

[50]A. Mödl, H. Robota, J. Segner, W. Vielhaber, M. C. Lin, and G. Ertl, Surf. Sci. **169**, L341 (1986).

[51]R. Schinke, Annu. Rev. Phys. Chem. **39**, 39 (1988).

[52]R. Gomer, in *Desorption Induced by Electronic Transition, DIET I*, edited by N. H. Tolk, M. M. Traum, J. C. Tully, and T. E. Madey, Springer Series in Chemical Physics (Springer, Berlin, 1983), Vol. 24, p. 40.

[53]A. R. Burns, E. B. Stechel, and D. R. Jennison, Phys. Rev. Lett. **58**, 250 (1987); in *Desorption Induced by Electronic Transition, DIET III*, edited by R. H. Stulen and M. L. Knotek, Springer Series in Surface Science (Springer, Berlin, 1988), Vol. 13, pp. 67–72; E. B. Stechel, D. R. Jennison, and A. R. Burns, *ibid.*, pp. 136–143.

[54]E. Hasselbrink (to be published).